ELSEVIER

International Journal of Mass Spectrometry 220 (2002) 137–143

International Journal of Mass Spectrometry

www.elsevier.com/locate/ijms

Photochemistry of $(NO)_n^-$ as studied by photofragment mass spectrometry

Tatsuya Tsukuda[a,b], Lei Zhu[a,1], Morihisa Saeki[a], Takashi Nagata[b,*]

[a] *Institute for Molecular Science, Myodaiji, Okazaki 444-8585, Japan*

[b] *Department of Basic Science, Graduate School of Arts and Sciences, The University of Tokyo, Komaba, Meguro-ku, Tokyo 153-8902, Japan*

Received 1 October 2001; accepted 15 February 2002

Abstract

Photofragmentation of $(NO)_n^-$ ($3 \leq n \leq 21$) in the energy range 2.7–3.6 eV (350–460 nm) results in the production of $(NO)_m^-$ with $m \geq 2$ and $NO_2^-\cdot(NO)_m$ with $0 \leq m \leq 2$. The photofragment yield spectra obtained for $n = 3$–7 display a broad and structureless band profile with successive blue-shift with increase in the cluster size, indicating that $(NO)_3^-$ behaves as a chromophoric core in the larger $(NO)_n^-$. The observed fragmentation patterns suggest that photoexcitation of the $(NO)_3^-$ chromophore is followed by direct dissociation into $(NO)_2^-$, solvent evaporation to form $(NO)_m^-$, and/or intracluster reactions to produce NO_2^-. (Int J Mass Spectrom 220 (2002) 137–143)

Keywords: Nitric oxide cluster anion; Photofragmentation; Disproportionation

1. Introduction

In the nitric oxide chemistry, such as the well-known third-order reaction $2NO + O_2 \rightarrow 2NO_2$, equilibrium between NO and N_2O_2 plays an important role for preparing the activated complexes. This comes mainly from the unique electronic properties of NO having an unpaired electron, which gives rise to the propensity for aggregation. Because of the large electron affinity of NO aggregates [1,2] and enhanced stabilities of the resultant NO cluster anions [1,3,4], the aggregation propensity is further emphasized in the reactions involving NO reduction, where reducing reagents provide excess electrons. In fact, the importance of an $N_2O_2^-$ or $N_2O_2^{2-}$ intermediate was suggested in the reduction of NO with CO to form N_2O at a CaO surface [5]. Turning to larger analogues, there have been several reports on the disproportionation reactions of $(NO)_3^-$. Grätzel et al. have investigated NO reduction processes in an aqueous solution using a pulse radiolysis technique, and determined the rate constant for the decay of $(NO)_3^-$ into $N_2O + NO_2^-$ [6]. Recently, Lugez et al. have measured IR spectra of ionic species produced by ≈5 K co-deposition of a Ne:NO sample with Ne atoms pre-excited by a microwave discharge [7]. On the basis of spectroscopic analysis of isotope-substituted $(NO)_3^-$ species, they concluded that *cis*, *cis*-$N_3O_3^-$ (**1** in Scheme 1) is formed in the neon matrix. They also found that photodestruction of *cis*, *cis*-$N_3O_3^-$ trapped in solid neon yields an $N_2O\cdots NO_2^-$ complex. As for the gas-phase cluster experiment, Yamaguchi et al. studied the dissociation

* Corresponding author. E-mail: nagata@cluster.c.u-tokyo.ac.jp

[1] Present address: Data Storage Institute, National University of Singapore, 10 Kent Ridge Crescent, Singapore 119260, Singapore.

1387-3806/02/$ – see front matter
PII S1387-3806(02)00769-8

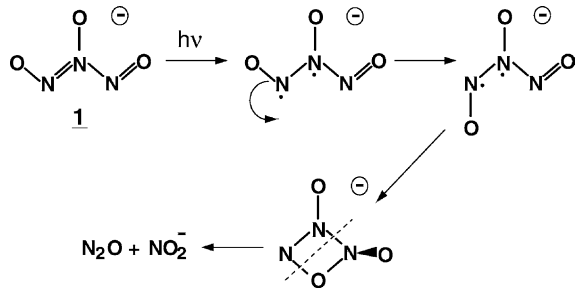

Scheme 1.

processes of $(NO)_n^-$ ($3 \leq n \leq 41$) in collision with a silicon surface [8]. They have detected an NO_2^- fragment produced via collision-induced disproportionation of $(NO)_3^-$ at the impact energy of ≈10 eV per molecule. Regarding the mechanism of the disproportionation reaction of $(NO)_3^-$, Snis and Panas theoretically proposed a possible decomposition pathway of *cis*, *cis*-$N_3O_3^-$ as depicted in Scheme 1 [9]. According to their CASPT2 calculations, the π–π^* transition at the excitation energy of 2.5 eV breaks the delocalized π system, which induces a conformational change of *cis*, *cis*-$N_3O_3^-$ into *trans*, *cis*-$N_3O_3^-$, then followed by NO_2 elimination.

In the present study, we investigated the photoproducts from $(NO)_n^-$ ($3 \leq n \leq 21$) in the energy range 2.7–3.6 eV (350–460 nm) using conventional photofragment mass spectrometry. The photofragment yield spectra of $(NO)_n^-$ were also obtained for $n = 3$–7, which provide information on the chromophore in $(NO)_n^-$. The purpose of the present study is (1) to identify the product channel of the unimolecular decomposition of photoexcited $(NO)_3^-$ in order to make an answer to the question whether or not the proposed disproportionation mechanism operates in an isolated $(NO)_3^-$, and (2) to give an insight into the mechanism of disproportionation reactions of NO aggregates trapping an excess electron.

2. Experimental

The schematic of the experimental apparatus is shown in Fig. 1. The apparatus consists of a negative-ion source and a collinear tandem time-of-flight

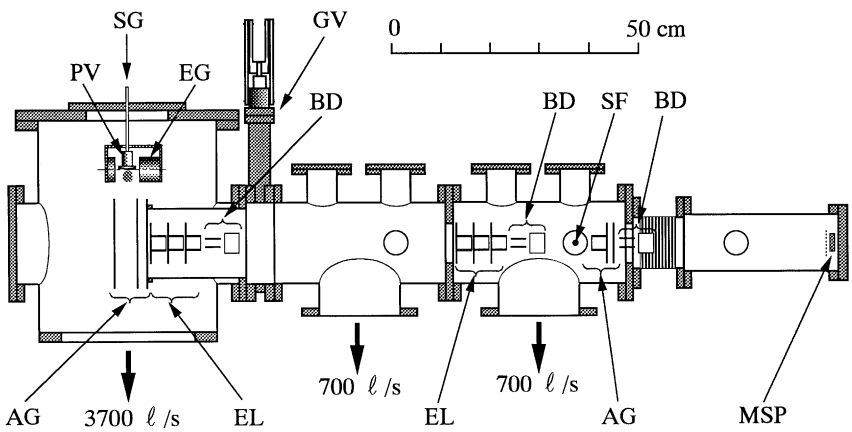

Fig. 1. Schematic of the experimental apparatus. AG: acceleration grids; BD: beam deflectors; EG: electron gun; EL: Einzel lens; MSP: microsphere plates; PV: pulsed valve; SF: spatial focus; SG: sample gas.

(TOF) mass spectrometer. The $(NO)_n^-$ clusters are generated via electron attachment to neutral NO clusters in an electron-impact ionized free jet [10]. The neutral NO clusters are prepared by pulsed supersonic expansion of a ≈1:4 mixture of NO and Ar gas at the stagnation pressure of 1–2 atm. In order to remove the impurities in the mixture, such as NO_2 and N_2O, the gas line is immersed in a slush bath of ethanol/liquid nitrogen maintained at ≈170 K. The pulsed free jet is crossed with a continuous beam of 250 eV electrons at the expansion region, where secondary slow electrons are efficiently produced. Within the ionized free jet, the slow electrons attach to the pre-existing $(NO)_N$ to form $(NO)_n^-$ cluster anions. The $(NO)_n^-$ clusters are extracted at ≈200 mm downstream the nozzle perpendicularly to the initial beam direction by applying a 1.5 kV high-voltage electric pulse and subjected to a TOF mass analysis. After mass selection of the anions of interest by time-of-flight, the output of a pulsed dye laser intersects the bunch of anions at the primary focus of the tandem mass spectrometer. Various photon energies of 2.7–3.6 eV are obtained by an excimer-pumped dye laser system, in which four different dyes are used to cover the whole spectral range studied. The photofragment ions, along with the remaining parent anions, are then collinearly accelerated by another 1.5 kV electric pulse. They are mass-analyzed during the propagation in the second TOF mass spectrometer, and detected by a microshere plate (El-Mul Z033DA) located at the end of the ≈50 cm flight tube. Data acquisition is achieved through a 500 MHz digitizing oscilloscope controlled via GPIB by LabView Virtual Instruments (National Instruments). Photofragment spectra are normalized to the laser fluence monitored by using a fast response pyroelectric detector (Molectron J3-09).

To make a reliable measurement of photofragment yield spectra with the present set-up, it is important to ensure the satisfactory overlap, both spatially and temporally, between the laser beam and the ion beam in the interaction region. This is accomplished by using an adjustable telescope system to expand the laser beam to get a more uniform intensity distribution. In order to avoid the occurrence of multiphoton processes, such as subsequent photofragmentation of product anions, the laser fluence is kept typically below ≈3 mJ cm^{-2}. In the whole spectral region the photofragment distributions are found to be almost independent of the laser fluence. For larger $(NO)_n^-$ a slight indication of multiphoton processes was observed but not significant. The data presented here were obtained by recording at least three sets of measurements, while for each TOF mass spectrum the signal was averaged for more than 300 individual laser shots.

3. Results

Fig. 2 shows the photofragment mass spectra of $(NO)_n^-$ $(3 \leq n \leq 21)$ recorded at the photon energy of 2.8 eV (440 nm). The observed fragment mass peaks are assigned to ions with the formula $(NO)_m^-$ $(m \geq 2)$, excepting those labeled by asterisks in Fig. 2.

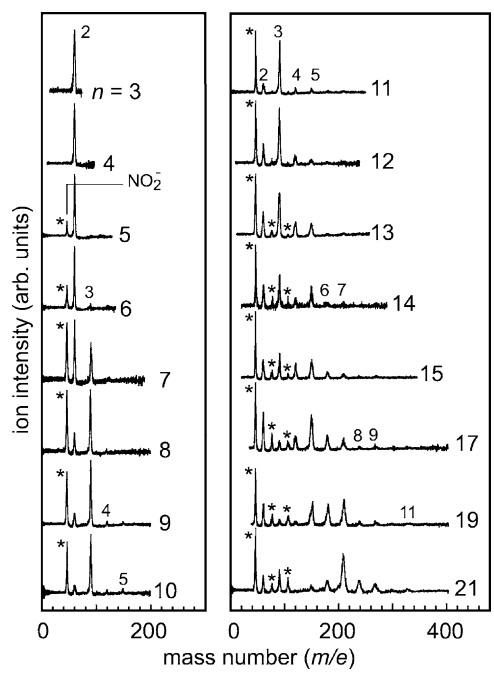

Fig. 2. Photofragment mass spectra of $(NO)_n^-$ $(3 \leq n \leq 21)$ recorded at the photon energy of 2.8 eV. Digits attached to the mass peaks correspond to the size m of $(NO)_m^-$ photofragments. The mass peaks assigned to $NO_2^- \cdot (NO)_m$ series with $0 \leq m \leq 2$ are labeled with asterisks.

The asterisked peaks are assignable to $NO_2^-\cdot(NO)_m$ species with $0 \leq m \leq 2$. Each fragmentation pattern does not change significantly as the excitation energy is varied in the range 2.7–3.6 eV. This allows us to extract the characteristics of the $(NO)_n^-$ photochemistry common in 350–460 nm from the photofragment mass spectra taken at 440 nm. As readily seen in Fig. 2, the fragmentation patterns display the following distinct features: (i) $(NO)_2^-$ production is the only photodestruction channel of $(NO)_3^-$; (ii) NO_2^- is produced only from $(NO)_n^-$ with $n \geq 5$; (iii) NO_2^- appears as a major photoproduct from $(NO)_n^-$ with $7 \leq n \leq 21$; (vi) the $(NO)_m^-$ photofragment distributions shift towards higher masses as the parent cluster size increases. These features are summarized in Fig. 3, where the branching fractions for NO_2^-, $(NO)_2^-$ and $(NO)_3^-$ productions are plotted against the parent cluster size for $3 \leq n \leq 10$.

The photofragment yield (PFY) spectra of $(NO)_n^-$ are obtained by integrating the intensities of all the photofragment signals as a function of the excitation energy. Fig. 4 depicts the PFY spectra of $(NO)_n^-$ ($3 \leq n \leq 7$), thus, obtained in the energy range 2.7–3.6 eV. Each PFY spectrum displays a broad and structureless profile with the maximum being located well below the vertical detachment energy (VDE) [11], which is defined as the energy required to remove the excess electron from an anion retaining its equilibrium geometry. The $(NO)_3^-$ spectrum possesses a relatively sharp profile centered at 2.9 eV, which is well represented by a Lorentzian function (not shown in Fig. 4). The spectral profiles of the $n \geq 4$ clusters resemble that of $(NO)_3^-$ except for a successively blue-shifted maximum (≈50 meV per cluster size) and an increasing width as the cluster size increases. The fact that the band maximum for each cluster size is located well below the VDE ensures that photodetachment process cannot make a significant contribution in the photodestruction process of $(NO)_n^-$. Under the assumption that photofragmentation is the one and only possible decay channel for the photoexcited $(NO)_n^-$, the PFY spectra can be regarded as the photoabsorption spectra of $(NO)_n^-$. In Fig. 4 also shown for comparison

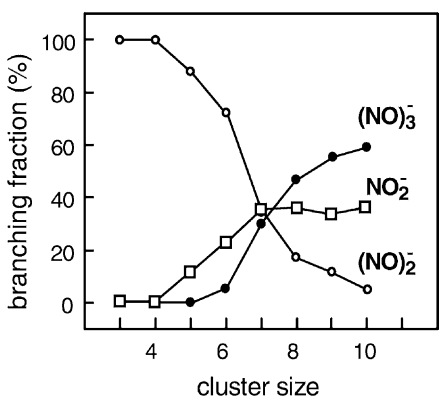

Fig. 3. Cluster-size dependence of branching fractions for the production of NO_2^- (squares), $(NO)_2^-$ (open circles) and $(NO)_3^-$ (filled circles) at the photon energy of 2.8 eV. Plots are made for the $3 \leq n \leq 10$ data for clarity.

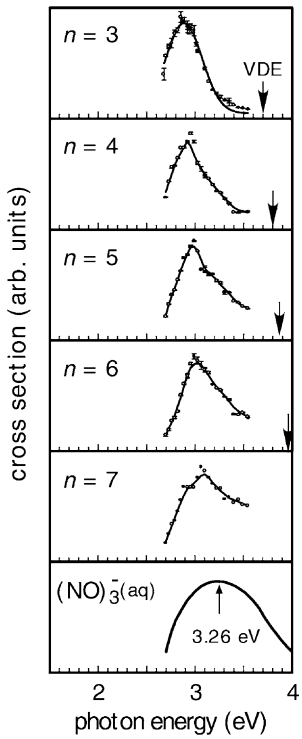

Fig. 4. Photofragment yield spectra of $(NO)_n^-$ ($3 \leq n \leq 7$). Arrows indicate the vertical detachment energies (VDEs) determined by photoelectron spectroscopy [11]. At the bottom panel, $(NO)_3^-$ photoabsorption spectrum in aqueous solution is reproduced from [6]. The solid curves are only for eye guide.

is the photoabsorption spectrum of $(NO)_3^-$ formed in an aqueous solution [6]. The comparison suggests the condensed-phase $(NO)_3^-$ spectrum as the asymptotic limit of the gas-phase $(NO)_n^-$ spectra with $n \rightarrow \infty$.

4. Discussion

4.1. Chromophoric core of $(NO)_n^-$

Previously, we have measured photoelectron spectra of $(NO)_n^-$, and determined VDEs of $(NO)_n^-$ in the range $2 \leq n \leq 7$ [11]. Based on the VDE measurement, in combination with ab initio calculations, we concluded that $N_3O_3^-$ is formed as the anionic core in the larger $(NO)_n^-$ prepared through the electron attachment to neutral $(NO)_N$. Hence, the larger $(NO)_n^-$ can be formulated as $N_3O_3^-\cdot(NO)_{n-3}$. The present finding, the similarity of photoabsorption bands of $(NO)_n^-$ $(4 \leq n \leq 7)$ to that of $(NO)_3^-$, not only reinforces the previous conclusion but also indicates that the $N_3O_3^-$ core acts as a chromophore for the photoabsorption in the $n \geq 4$ clusters. As seen in Fig. 4, the $(NO)_n^-$ spectral profile becomes much closer to the aqueous $(NO)_3^-$ photoabsorption band with increase in the cluster size. This suggests that $(n - 3)$ NO molecules play merely a role of solvent in $(NO)_n^-$, being consistent with the representation $N_3O_3^-\cdot(NO)_{n-3}$. Under these circumstances, photoexcitation is initially confined to the $N_3O_3^-$ moiety, followed by several decay processes, such as direct dissociation of the chromophore, energy dissipation into solvents and/or secondary chemical reactions within clusters.

The next issue to address concerns the chemical identity of the $N_3O_3^-$ chromophore. We have proposed five possible forms of stable structures for $N_3O_3^-$ by MP2/6-31+G* calculations [11]: two normal chain $[ONNONO]^-$ and three branched chain $[ONN(O)NO]^-$ structures. MP4 energies of these structures were calculated with the geometries optimized at the MP2/6-31+G* level. Among those isomeric structures *all cis*-branched chain with C_{2v} symmetry, that is the *cis*, *cis*-$N_3O_3^-$ species, was found to be most stable. The MP4 energies of all the remaining structures lie within 1 eV above the lowest energy: for example, *all trans*-normal chain is only 0.3 eV higher in energy than *cis*, *cis*-$N_3O_3^-$. This allows of the possibility for the coexistence of several isomers in $N_3O_3^-$. Recently, Lugez et al. have examined the IR spectra of $(NO)_3^-$ prepared in a neon matrix [7]. With the aid of B3LYP density functional calculations predicting the isotope-shift patterns of fundamental vibrational frequencies, they have identified $(NO)_3^-$ trapped in solid neon exclusively as *cis*, *cis*-$N_3O_3^-$. They also found that *cis*, *cis*-$N_3O_3^-$ undergoes photodestruction by the irradiation of <2.95 eV photons, leading to the formation of an $N_2O\cdots NO_2^-$ complex. The identification of *cis*, *cis*-$N_3O_3^-$ in solid neon was further supported by theoretical study [9], where the combination of B3LYP density functional theory and the wave function-based CASPT2 method was used to predict the vertical electron excitation energies and vertical electron detachment energies for *cis*, *cis*-$N_3O_3^-$. The calculated VDE value (3.73 eV) agrees excellently with the experimental one (3.70 ± 0.02 eV) determined by photoelectron spectroscopy [11]. Looking over the PFY results (Fig. 4) again in conjunction with the findings reported previously—especially the occurrence of photodestruction of *cis*, *cis*-$N_3O_3^-$ by <2.95 eV photons [7]—and considering the excellent agreement of theoretical and experimental VDE values [9,11], we infer that the $N_3O_3^-$ chromophoric core discussed here also takes on the *cis*, *cis*-$N_3O_3^-$ form. Although we cannot completely rule out the possibility for other $N_3O_3^-$ isomers coexisting in our cluster beam, it is rather unlikely that the most stable isomer, *cis*, *cis*-$N_3O_3^-$, is not formed as a dominant species under the preparation conditions of our cluster beam.

4.2. Photochemistry of $(NO)_n^-$

Within the framework of the above discussion, photodissociation of $(NO)_3^-$ provides a good starting-point for discussion. It is obvious from the results shown in Fig. 2 that photodissociation of

$(NO)_3^-$ proceeds as

$$(NO)_3^- + h\nu \rightarrow (NO)_2^- + NO. \quad (1)$$

The broad and structureless profile of the PFY spectrum for $(NO)_3^-$ indicates direct dissociation of $(NO)_3^-$ upon photoexcitation. Considering the chemical identity of $(NO)_3^-$ as *cis*, *cis*-$N_3O_3^-$, process (1) is rewritten more explicitly as

$$cis, cis\text{-}N_3O_3^- + h\nu \rightarrow cis\text{-}ONNO^- + NO, \quad (1')$$

where the endothermicity is estimated to be 1.20 eV by B3LYP calculations [9]. Process (1′) is a striking contrast to the photodestruction process of *cis*, *cis*-$N_3O_3^-$ in a rare-gas matrix, where $N_2O + NO_2^-$ is found to be the photoproduct channel [7]. To reconcile the apparent discrepancy between the gas- and condensed-phase phenomena, we focus attention on the mechanism of NO_2^- production in the larger $(NO)_n^-$ with $n \geq 5$ [finding (ii)]. Since $N_3O_3^-$ plays a chromophoric role in the larger $(NO)_n^-$, process (1′) occurs as an early time dynamics in photoexcited $(NO)_n^-$. The *cis*-$ONNO^-$ fragment, produced within the cluster via the direct dissociation of the $N_3O_3^-$ core, further reacts with solvent NO molecules through either of the following processes:

$$cis\text{-}ONNO^- + NO \rightarrow N_2O + NO_2^-, \quad (2)$$

$$cis\text{-}ONNO^- + (NO)_2 \rightarrow N_2O + NO_2^- + NO. \quad (3)$$

Both processes (2) and (3) are exothermic with $\Delta H = -2.32$ and -2.25 eV, respectively. These ΔH values are estimated based on the B3LYP/6-311+G(d) energy of *cis*-$ONNO^-$ [9]. As for process (2), recent theoretical calculations with unrestricted B3LYP/cc-pVTZ level proposed two possible pathways with a quite low energy barrier [12], one of which is shown in Scheme 2. Process (3) is likely to proceed in the presence of neutral NO pairs in $(NO)_n^-$. There is, of course, no reason to exclude the possibility that the dissociated system, *cis*-$ONNO^- + NO$, in turn react inside the solvent cage to produce $N_2O + NO_2^-$.

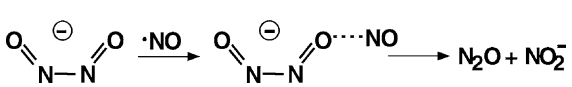

Scheme 2.

We will discuss the proposed mechanism of NO_2^- production in terms of the size-dependence of the branching fractions (Fig. 3). The increase in the NO_2^- fraction with the cluster size is ascribable to the increase in the number of solvent NO molecules which take part in processes (2) and (3). The rapid drop in the $(NO)_2^-$ fraction arises possibly from the consumption of photoproduct $ONNO^-$ via processes (2) and/or (3), and from the caging of otherwise dissociating photoexcited $(NO)_3^-$. The caging process in turn makes an increasing contribution to $(NO)_3^-$ production as the cluster size increases:

$$\begin{aligned} &N_3O_3^- \cdot (NO)_{n-3} + h\nu \\ &\rightarrow [N_2O_2^- \cdots NO]^* \cdot (NO)_{n-3} \\ &\rightarrow N_3O_3^- + (n-3)NO, \end{aligned} \quad (4)$$

where the energy deposited in the chromophore is large enough to evaporate almost all the solvent NO neutrals. Once either process (2) or (3) occurs, a sizable amount of excess energy is stored within the cluster due to the large exothermicity of ≈2.3 eV. The excess energy is consumed inevitably to boil off the solvent NO, leading to the production of relatively small members of $NO_2^- \cdot (NO)_m$ with dominant population at $m = 0$. This is always the case in $(NO)_n^-$ cluster with $5 \leq n \leq 21$.

From the above considerations, we reach to the conclusions that (1) the 350–460 nm photodissociation of $(NO)_3^-$ having *cis*, *cis*-$N_3O_3^-$ structure leads directly to $(NO)_2^- + NO$ channel, which causes subsequent intracluster reactions in larger $(NO)_n^-$ with $n \geq 5$, and that (2) NO_2^- is formed via the intracluster reaction between solvent NO and *cis*-$ONNO^-$ formed in the photodissociation of $N_3O_3^-$ chromophore. These inferences lead us to say further that disproportionation reaction of $(NO)_3^-$, $(NO)_3^- \rightarrow N_2O + NO_2^-$, proceeds via the $(NO)_2^- \cdots NO$ intermediate, which is prepared efficiently in the presence of third body, such as NO neutrals in $(NO)_n^-$, inert surroundings in rare-gas matrices, or surface atoms on catalytic interfaces.

Acknowledgements

This work was supported in part by a Grant-in-Aid for Scientific Research from the Ministry of Education, Culture, Sports, Science and Technology (MEXT) under Grant no. 11166217.

References

[1] L.A. Posey, M.A. Johnson, J. Chem. Phys. 88 (1988) 5383.
[2] A. Snis, I. Panas, Mol. Phys. 91 (1997) 951.
[3] A. Snis, I. Panas, Chem. Phys. 221 (1997) 1.
[4] K. Hiraoka, S. Fujimaki, K. Aruga, J. Phys. Chem. 98 (1994) 8295.
[5] F. Acke, I. Panas, D.J. Strömberg, Phys. Chem. 101 (1997) 6484.
[6] V.M. Grätzel, S. Taniguchi, A. Henglein, Ber. Bunsenges. Physik. Chem. 74 (1970) 1003.
[7] C.L. Lugez, W.E. Thompson, M.E. Jacox, A. Snis, I. Panas, J. Chem. Phys. 110 (1999) 10345.
[8] H. Yamaguchi, Y. Fukuda, H. Yasumatsu, A. Terasaki, T. Kondow, private communication.
[9] A. Snis, I. Panas, Chem. Phys. Lett. 305 (1999) 285.
[10] M.A. Johnson, W.C. Lineberger, in: J.M. Farrar, W.H. Saunders (Eds.), Techniques of Chemistry, Vol. 20, Wiley, New York, 1988, p. 591.
[11] T. Tsukuda, M. Saeki, L. Zhu, T. Nagata, Chem. Phys. Lett. 295 (1998) 416.
[12] M.A. Vincent, L.D. Salsi, I.H. Hillier, Chem. Phys. Lett. 314 (1999) 138.